ACS Catalysis

RESEARCH ARTICLE

pubs.acs.org/acscatalysis

Aerobic Oxidation of Hydrocarbons Catalyzed by Mn-Doped Nanoporous Aluminophosphates (III): Propagation Mechanism

Luis Gómez-Hortigüela,* Furio Corà,* and C. Richard A. Catlow

Department of Chemistry, 20 Gordon Street, University College London, WC1H 0AJ London, United Kingdom

Supporting Information

ABSTRACT: We apply electronic structure methods based on hybrid-exchange DFT functionals under periodic boundary conditions to study the catalytic aerobic oxidation of hydrocarbons in Mn-doped aluminophosphates. In particular, we focus on the mechanism of the *propagation* reactions. Hydrocarbon oxidation is achieved via a succession of H abstraction, O_2 addition, and desorption reactions occurring on $Mn^{III}\cdots OX$ complexes (X = H, CH_2CH_3, or OCH_2CH_3). The complexes $Mn^{III}\cdots OH$ and $Mn^{III}\cdots OCH_2CH_3$ result from the *decomposition* of CH_3CH_2OOH by preactivated Mn^{II} sites, whereas $Mn^{III}\cdots OOCH_2CH_3$ is formed in *preactivation* or *propagation* routes. The radical nature of the oxo-type ligands (OX) allows for the homolytic H abstraction from new hydrocarbon molecules, leading to XO−H (HO−H, CH_3CH_2O−H and CH_3CH_2OO−H) and to $CH_3CH_2\cdot$ radicals that are stabilized by interaction with the H atoms transferred. Subsequent stereospecific O_2 additions yield free peroxo radicals $CH_3CH_2OO\cdot$ that undergo a propagation subcycle to produce further CH_3CH_2OOH; these hydroperoxide molecules re-enter the oxidation cycle by reacting with Mn^{II}. The different H abstraction ability of the $Mn^{III}\cdots OX$ complexes is related to the stability of the oxo radicals that act as ligands. Our results demonstrate that the role of the Mn sites in the propagation reactions is to stabilize the oxo radicals by forming complexes, but no redox process involving Mn takes place in this stage of the reaction; Mn^{III} is the only active species throughout the propagation steps.

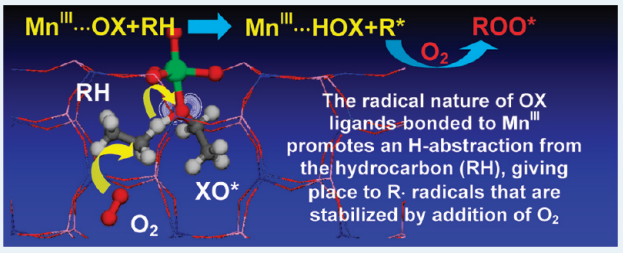

KEYWORDS: oxidation, heterogeneous catalysis, nanoporous aluminophosphates, zeolites, molecular modeling, aerobic, reaction mechanism

INTRODUCTION

Terminal oxi-functionalization of saturated hydrocarbons represents a major challenge in contemporary catalytic chemistry, especially if O_2 is to be used as oxidant. In past years, an intensive effort has been devoted to finding efficient heterogeneous selective oxidation catalysts able to sustain the aerobic selective oxidation process on an industrial scale. Crystalline nanoporous aluminophosphate materials (AlPOs),[1] which are zeolite-like materials in which silicon ions are replaced by phosphorus and aluminum, can easily accommodate framework substitutions of both Al and P, leading to acid, redox, and even bifunctional catalysts. In particular, Al can be replaced by transition metal cations, such as Co, Mn, and Fe, to produce redox catalysts,[2−9] which have been demonstrated to be very efficient in a large number of oxidation reactions using O_2 as the oxidant.[8−20]

The aerobic oxidation of cyclohexane catalyzed by MnAPO-5, a Mn-doped aluminophosphate with the AFI framework structure, has been the subject of in-depth mechanistic experimental investigations by Iglesia and co-workers.[15] Experimental evidence demonstrates the occurrence of a free-radical mechanism when Co-, Fe-, and Mn-containing AlPOs are used as catalysts;[8,15,21] however, experiment alone provides direct information on a subset only of the reaction intermediates. The availability of reliable computational models for the catalysts enables us to investigate this mechanism by contemporary electronic-structure methods, providing complementary data to experiments for mechanistic studies.

In a previous communication, we reported a summary of the complete reaction mechanism for the aerobic oxidation of ethane catalyzed by Mn-doped AlPOs,[22] in which we showed that the main catalytic cycle involves the simultaneous presence of Mn^{II} and Mn^{III} sites, each with a particular role along the reaction pathway. We proposed a *preactivation* step, in which the original Mn^{III} sites present in the calcined catalyst are transformed in Mn^{II} and Mn^{III}−peroxo complexes, both required for the subsequent *propagation* reactions.[23] We demonstrated that the *decomposition* of the hydroperoxide can take place only through reduced Mn^{II} sites, which are produced through the preactivation step.

In addition, we observed that the decomposition of CH_3CH_2OOH can take place through two alternative mechanistic routes: depending on the stereochemistry of the CH_3CH_2OOH adsorption on the Mn^{II} active site, CH_3CH_2OOH decomposition can yield either $Mn^{III}\cdots OCH_2CH_3$ and H_2O or $Mn^{III}\cdots OH$ and CH_3CH_2OH, resulting in the oxidation of the Mn sites.[24] It is

Received: August 2, 2011
Revised: September 14, 2011
Published: September 19, 2011

ACS Publications © 2011 American Chemical Society

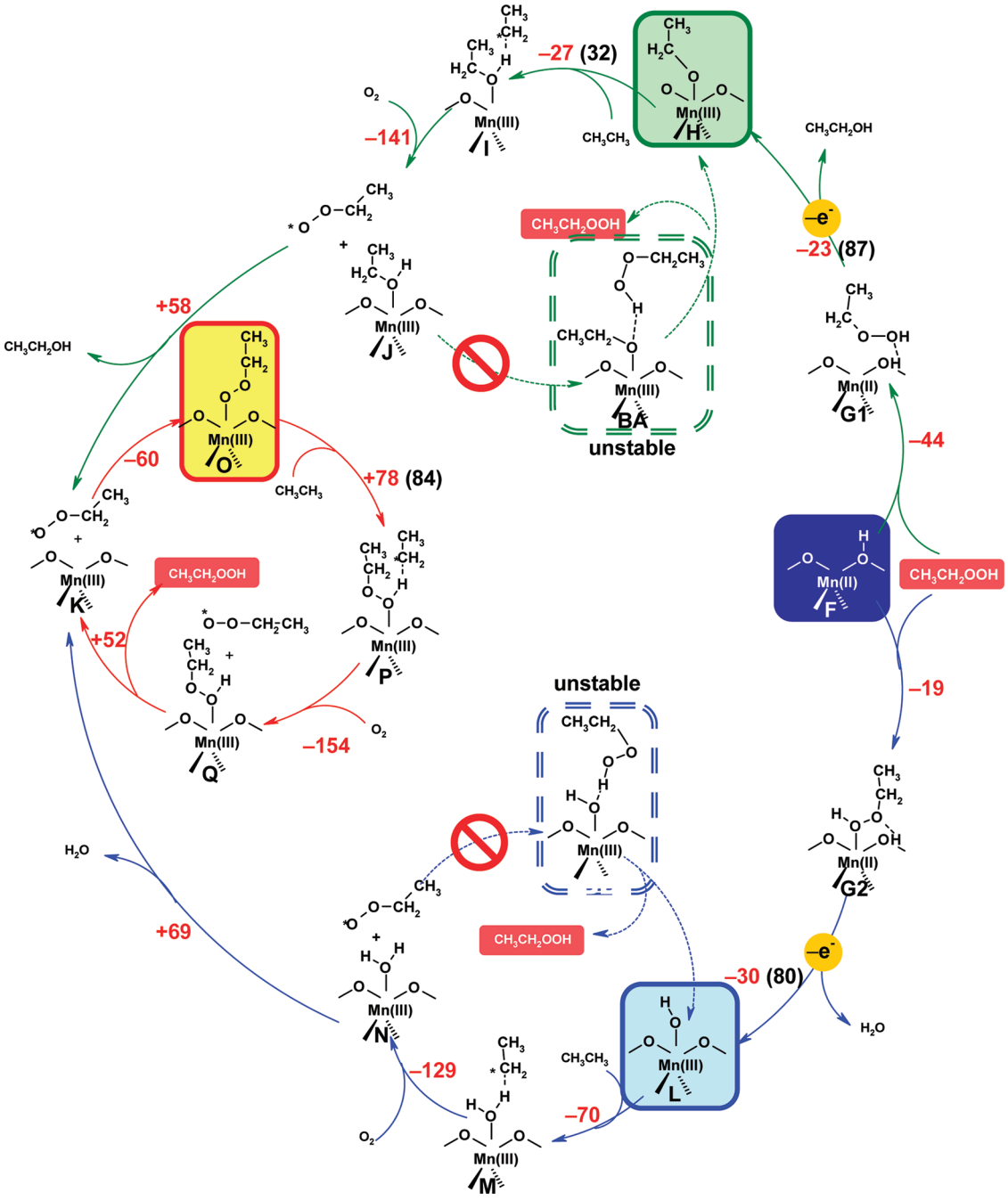

Figure 1. Scheme of the propagation reactions studied in this work. Enthalpies (in red) and activation energies, if any (in black and between brackets) are given in kJ/mol.

from these Mn^{III} complexes with oxo-type ligands ($Mn^{III}\cdots OCH_2CH_3$ and $Mn^{III}\cdots OH$) that the propagation reactions take place. The radical nature of the oxo-type ligands is responsible for the activation of new hydrocarbon molecules by means of H-transfer reactions to the radical O atom. These propagation reactions will finally yield $Mn^{III}\cdots OOCH_2CH_3$ complexes, which also are a product of the preactivation step, and from which new propagation reactions can occur. An in-depth analysis of the preactivation (I) and the hydroperoxide decomposition (II) steps has already been reported.[23,24] In this work, we now focus on the propagation reactions, which activate new hydrocarbon molecules and transform them into the oxidation products CH_3CH_2OH and H_2O and into further CH_3CH_2OOH that will sustain the overall oxidation cycle. The termination (*regeneration*) reactions will be covered in similar depth in the final paper in this series.[25]

COMPUTATIONAL METHODOLOGY

We use ethane (CH_3CH_3) as the hydrocarbon and Mn-doped AlPO-5 (MnAPO-5) as the catalyst; for details of the methodology, the reader is referred to refs 23 and 24. The Mn-doped AFI framework is described with periodic boundary conditions, using 1 crystallographic unit cell and *P*1 space group. One Al^{3+} ion per

dx.doi.org/10.1021/cs200401f |*ACS Catal.* 2011, 1, 1487–1497

AFI unit cell is substituted with Mn^{3+} in a tetrahedral position. We have performed density functional theory calculations, as implemented in the program CRYSTAL,[26] using the hybrid-exchange functional B3LYP. Selected reaction steps have also been studied using the B3LYP+D functional, including the empirical correction for dispersion proposed by Grimme.[27,28] Since both reagent and product molecules are contained in the zeolitic pores, we found the dispersion correction to remain roughly constant over the reaction steps, leaving a negligible contribution of less than 5 kJ/mol to the reaction energies.[24] For this reason, only uncorrected B3LYP results are discussed in the paper.

The computational methodology applied allowed us to obtain the energy profile for each elementary step along the selected reaction coordinate, from which the transition states and the correspondent activation energies were identified. The approximate transition state (TS) identified in this constrained search was very close to that obtained using second-derivative-based methods, in both geometry (to within the step size chosen) and energy (usually less than 4 kJ/mol). Fully optimized configurations for reactants and products were used to find reaction enthalpies for each elementary step.

RESULTS

For the sake of clarity and consistency, all our studies use the same labels for the intermediates involved, as introduced in previous works of the series.[22−24] Preactivation of the initial Mn^{III}-AFI catalysts in the presence of O_2 and the hydrocarbon (CH_3CH_3) yields the reduced form of the catalyst (Mn^{II}-AFI (**F**)), the hydroperoxide intermediate (CH_3CH_2OOH), and a complex between Mn^{III} and a peroxo radical ($Mn^{III}\cdots OOCH_2CH_3$, **O**).[23] The decomposition of the hydroperoxide intermediate CH_3CH_2OOH assisted by Mn^{II} yields complexes of Mn^{III} with alkoxy ($CH_3CH_2O\cdot$) or hydroxy ($HO\cdot$) radicals, $Mn^{III}\cdots OCH_2CH_3$ (**H**) or $Mn^{III}\cdots OH$ (**L**).[24] In the present study, we focus on the evolution of the three $Mn^{III}\cdots OX$ complexes, which have in common a radical O-based donor ligand, namely, $Mn^{III}\cdots OCH_2CH_3$ (**H**), $Mn^{III}\cdots OH$ (**L**), and $Mn^{III}\cdots OOCH_2CH_3$ (**O**). The $Mn^{III}\cdots OX$ complexes are responsible for the activation of new hydrocarbon molecules through H-transfer reactions, leading to a series of propagation reactions that will lead to the formation of the oxidation products (CH_3CH_2OH and H_2O) and to further hydroperoxide intermediate (CH_3CH_2OOH). Hereafter, the chain CH_3CH_2 will be denoted as R because the mechanisms we propose will be general for saturated hydrocarbons.

The complete set of reactions studied in this work are summarized in Figure 1. Intermediates **H**, **L**, and **O** produced in earlier stages of the reaction[23,24] are highlighted as shaded squares in Figure 1. All three complexes are more stable when the Mn^{III} and the oxo radical have opposite spins. Results will be presented in different subsections, considering the evolution of $Mn^{III}\cdots OR$ (**H**), $Mn^{III}\cdots OH$ (**L**), and $Mn^{III}\cdots OOR$ (**O**) complexes.

A. Propagation from $Mn^{III}\cdots OR$ (H → I → J → K). *A.1. H Transfer from RH to $Mn^{III}\cdots OR$ (**H** → **I**).* As explained in our previous work,[24] the most stable mode of adsorption of the hydroperoxide intermediate (ROOH) on Mn^{II} sites involves the formation of a strong H bond between the framework proton and the terminal O atom in ROOH and leads to the formation of the $Mn^{III}\cdots OR$ complex, **H**. The radical-like nature of this RO· ligand allows a propagation reaction to take place through H transfer from a new hydrocarbon molecule (RO· + RH → ROH + R·), saturating the ethoxo radical RO· and forming an ethanol molecule ROH. The energy diagram for this reaction is shown in Figure 2 (top); the reaction coordinate was set as the distance between the H atom in ethane that will be transferred and the radical O atom in RO·. An increase in the energy is observed as the H atom from the hydrocarbon approaches the radical O, giving an activation energy of 32 kJ/mol (Figure 3, top). Simultaneously, the C−H bond (also displayed in Figure 2, top, in blue) is elongated and eventually broken (after the transition state), leading to the formation of an ethyl radical R· and an ROH molecule that remains bonded to Mn. This H transfer has a reaction enthalpy of −27 kJ/mol. Figure 2, bottom shows the evolution of the spin polarization of the different species along the reaction coordinate. We observe that the spin of Mn (red line) is not modified upon this H transfer and remains as 3.83, which corresponds to Mn^{III}, showing that no redox process involving Mn takes place in this step. The H transfer involves a homolytic dissociation of the C−H bond in the hydrocarbon, which results in the formation of a radical species, as shown by the change in the spin of the C atom from 0 to −1 (green line). Simultaneously, the initial unpaired electron localized on the O atom of the RO ligand in $Mn^{III}\cdots OR$ (**H**) disappears as a result of the formation of a closed-shell species (ROH) (pink line).

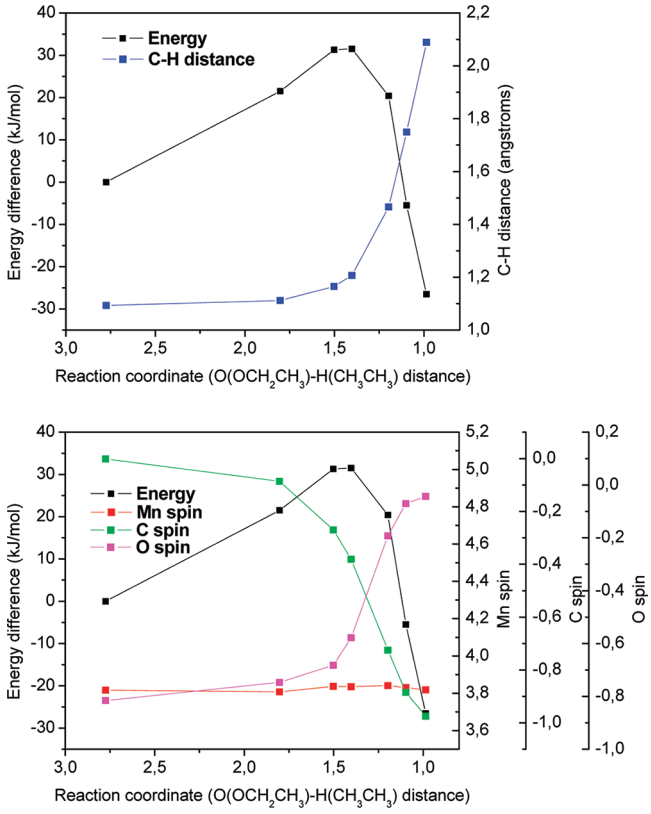

Figure 2. Top: Energy diagram (black line) and evolution of the C−H distance (blue line) along the reaction coordinate (represented as the distance between a H atom in CH_3CH_3 and the O atom in OCH_2CH_3 ($O(OCH_2CH_3)-H(CH_3CH_3)$ distance) for the H transfer reaction from ethane to the ethoxo ligand bonded to Mn^{III} (**H** → **I**). Bottom: Energy diagram (black line) and evolution of the C (green line), O (pink line), and Mn (red line) spin along the reaction.

dx.doi.org/10.1021/cs200401f |ACS Catal. 2011, 1, 1487–1497

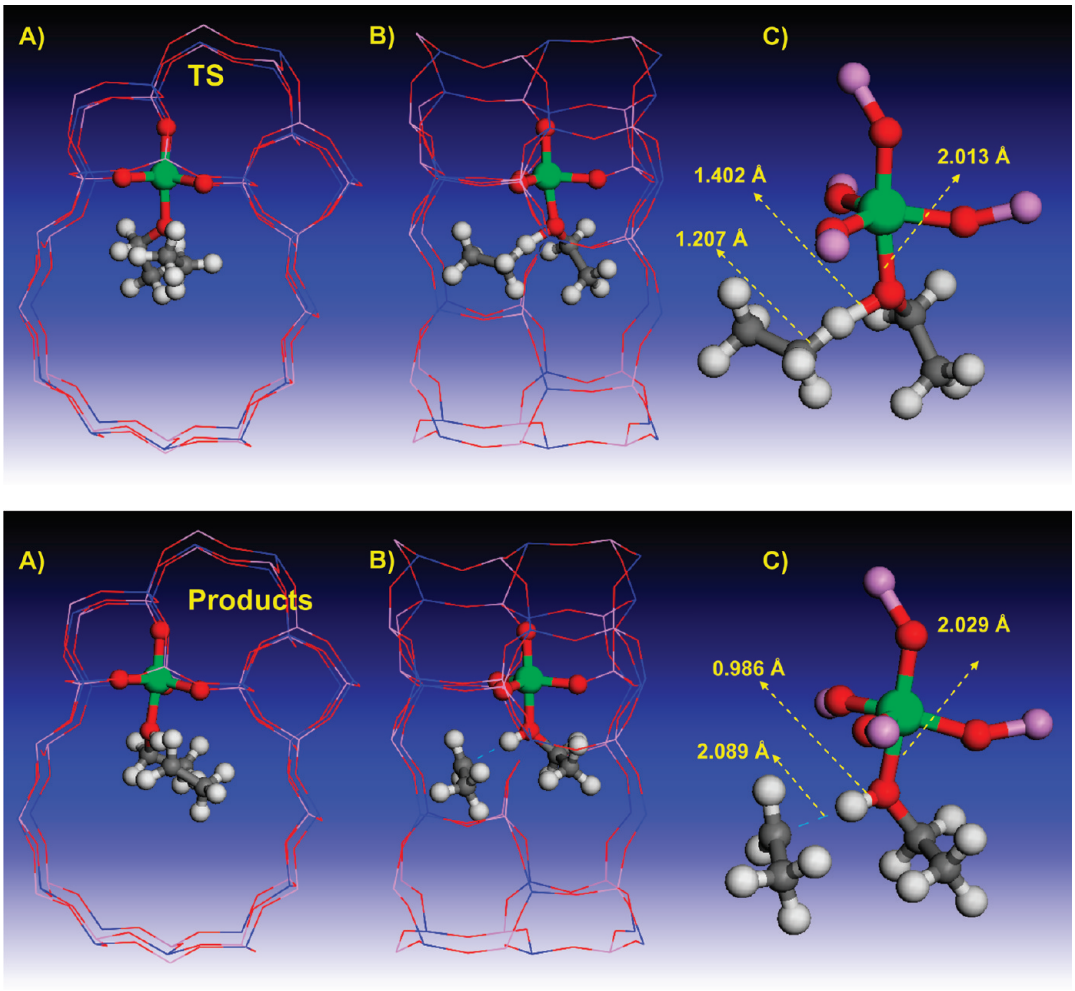

Figure 3. Two views (A and B) and detail (C) of the structure of the transition state ($\mathbf{TS_{H\rightarrow I}}$) (top) and of the products (**I**) (bottom) for the H transfer reaction from ethane to the ethoxo ligand bonded to Mn^{III} (**H** → **I**), giving place to a molecule of ethanol and an ethyl radical.

The molecular structures of the transition state (TS) and products (**I**) are shown in Figure 3 (top and bottom, respectively), and the spin density maps for the reactants, TS, and products are displayed in Figure 4 (left, middle, and right, respectively). In the reactants, the α spin density (displayed in red) is localized on the Mn atom, and the β spin density (displayed in blue) is localized on the O atom of the RO· ligand, showing the radical nature of this ligand (Figure 4-left). In the TS, we observe that the H atom is being transferred between the C and the O atoms (Figure 3, top); the C atom retains a quasi-tetrahedral environment in the TS. The β spin density shifts in the direction opposite to the H, and in the TS, it is shared between the C atom of RH (which is an incipient radical) and the O atom in the RO· ligands (Figure 4-middle), consistent with the homolytic dissociation of the C−H bond and the formation of an O−H bond.

The H atom has very low spin density in the transition state, indicating that it mediates the radical transfer from O to C, but does not itself become spin-polarized. The structure of the resulting products (**I**) (Figure 3, bottom) shows the formation of an R· species. A strong interaction between the radical and the H atom that has been transferred to ROH is observed (highlighted by a dashed blue line), indicating that the resulting ethyl radical is not free inside the channel, but is associated with the ROH ligand formed, which in turn is bonded to Mn. The radical nature of the R· species is clear from the spin density maps of the products (Figure 4, right).

A.2. O_2 Addition to R· (***I*** → ***J***). The ethyl radical R· (**I**) is a very reactive species, and in the presence of molecular O_2, it reacts rapidly to form the peroxo radical ROO·. As observed in the preactivation,[23] addition of O_2 to the ethyl radical takes place without significant activation barriers. Due to the molecular configuration of **I**, where R· interacts with the H atom in ROH, this O_2 attack can take place only from the opposite side of the CH_2 plane (from the left side in Figure 3, bottom, B), since an attack from the opposite side is sterically impeded by the ROH ligand bonded through Mn to the framework. This stereospecific O_2 addition is very exothermic (−141 kJ/mol), and gives rise to a peroxo free-radical (ROO·) located in the middle of the channel (**J**) (Figure 5). The addition of O_2 causes the R· radical to separate from the H atom of ROH, yielding a free radical (ROO·) that is not chemisorbed on the framework. The spin evolution in this step shows that the spin polarization of the C atom is transferred to O_2 as it binds: the C spin varies from −1 to 0; the spin polarization is then shared by the two molecular O atoms in ROO·, which reduce their initial spin of 1 (in the triplet ground state of molecular O_2) to 0.7 and 0.3, higher on the terminal O atom (Figure 5, right).

dx.doi.org/10.1021/cs200401f |*ACS Catal.* 2011, 1, 1487–1497

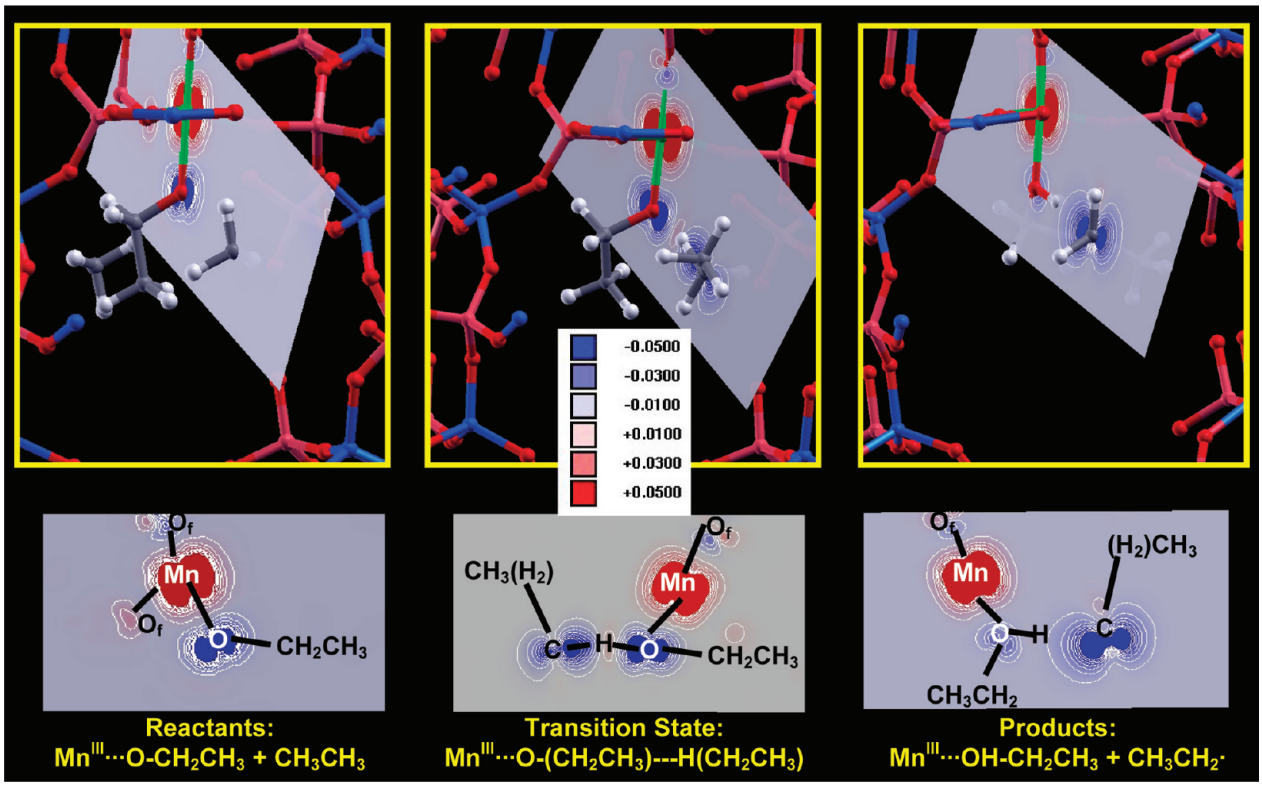

Figure 4. Spin density maps of the reactants (left), transition state ($TS_{H\rightarrow I}$, middle), and products (**I**, right); β and α spin densities are displayed in blue and red, respectively. White lines indicate isodensity lines. For the sake of clarity, the same maps are displayed at the bottom without the atoms.

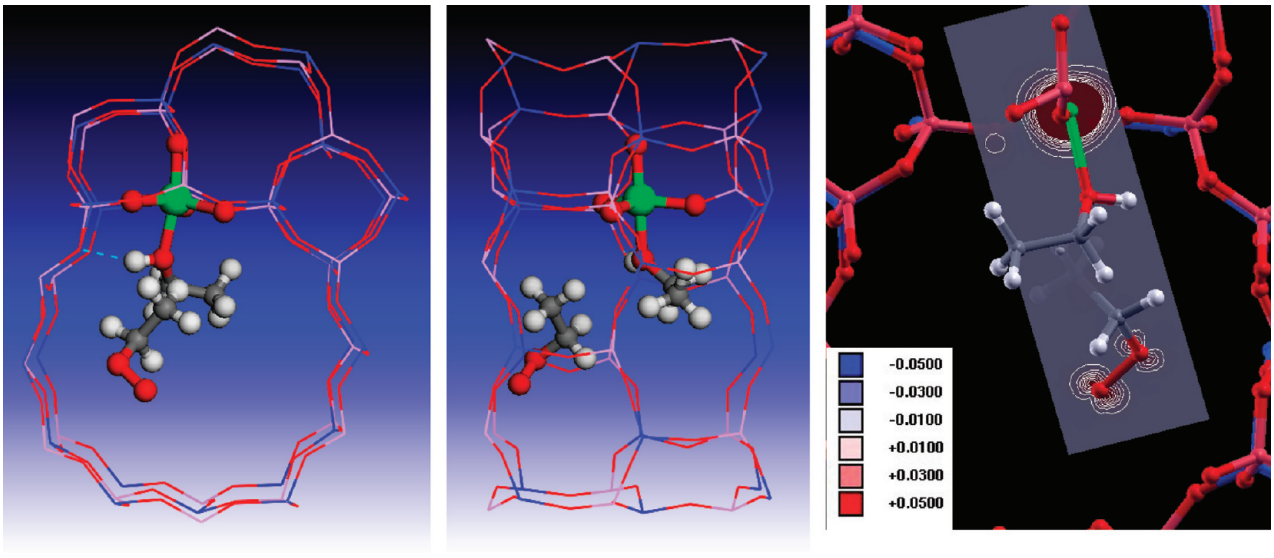

Figure 5. Two views of the molecular structure (left and middle) and spin density maps (right) of the products resulting from the insertion of O_2 to the ethyl radical, $Mn^{III}\cdots OHCH_2CH_3$ + free $CH_3CH_2OO\cdot$ (**J**).

The presence of the peroxo radical intermediate enables, in principle, a propagation subcycle from which further ROOH could be produced (subcycle **J** → **BA** → **H** → **I** → **J** in Figure 1). This subcycle is initiated by a H transfer from the recently formed ROH ligand to the free peroxo radical in **J**, leading to the formation of the hydroperoxide intermediate (ROOH) and again the $Mn^{III}\cdots OR$ complex (**BA**). Subsequent desorption of the ROOH intermediate from **BA** would yield **H** and close a propagation subcycle, whose net reaction is the production of one hydroperoxide ROOH molecule from RH and O_2 (i.e., RH + O_2 → ROOH). However, our calculations showed that the **BA** intermediate is very unstable and possibly not even a minimum in the potential energy surface; geometry optimizations always reverted in the H atom being transferred back to the RO· radical

dx.doi.org/10.1021/cs200401f |*ACS Catal.* 2011, 1, 1487–1497

Table 1. Calculated C−H and O−H Bond Energies in Ethane, Ethanol, Water and Ethyl Hydroperoxide[a]

Molecule	H abstraction	Bond energy	ΔH H-abstract	Ea H-abstract	ΔH R· desorption	ΔH O_2 addition	ΔH XOH desorption
CH_3CH_3	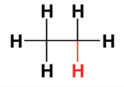	+454	---	---	---	---	---
H_2O		+500	–27	32	22	–129	+69
CH_3CH_2OH	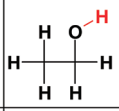	+442	–70	None	14	–141	+58
CH_3CH_2OOH	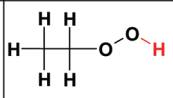	+362	+78	84	1	–154	+52

[a] The bond examined is displayed in red−, and corresponding enthalpies (and activation energies) for the H abstraction from a hydrocarbon molecule (**H** → **I**, **L** → **M**, and **O** → **P**), desorption of the R· radical from the ligand, O_2 addition to R· (**I** → **J**, **M** → **N**, and **P** → **Q**), and XOH desorption (**J** → **K**, **N** → **K** and **Q** → **K**). Bond energies were defined as RH → R· + H· and were calculated with the same level of theory (DFT-B3LYP). All energies are expressed in kJ/mol.

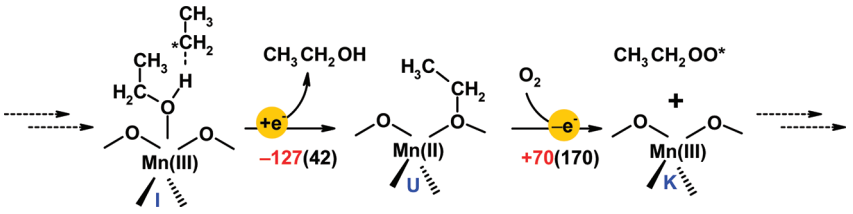

Figure 6. Top: Scheme of the reactions involving the formation of a complex between Mn^{II} and the ethyl radical by approaching of this to a (nearest-neighbor to Mn) framework O (**U**) and the subsequent attack of O_2 to the ethyl ligand to form the peroxo derivative (**K**). Bottom: energy diagram for this route.

to yield **J**, thus ruling out the occurrence of this alternative propagation mechanism. The instability of the **BA** intermediate is due to the much lower stability of RO· compared with ROO· radicals, as shown by the calculated O−H bond energy of ROH (442 kJ/mol) compared with ROOH (362 kJ/mol; see Table 1).

The most probable evolution of intermediate **J** is therefore the desorption of ROH from Mn^{III}, which releases the Mn active site; this process is endothermic, with a reaction enthalpy of +58 kJ/mol; it leads to a new intermediate, **K**, where we have a free peroxo radical (ROO·) and the Mn^{III} site.

*A.3. Bonding of R· to Framework O (**I** → **U** → **K**).* An alternative reaction path to that discussed in section A.2 may occur, starting from intermediate **I**. At this stage, we have one ethyl radical R· stabilized by a strong interaction with the H atom in the ROH ligand. As an alternative to the addition of O_2 discussed in the previous section, this radical could be stabilized by bonding to a framework O atom nearest neighbor to Mn, yielding intermediate **U** and resulting in the transfer of the unpaired electron in R· to Mn. This process should, in principle, be favored by the disappearance of the spin-polarization in R· and the reduction of Mn^{III} to Mn^{II}, the stable oxidation state of Mn in AlPOs (Figure 6). This process was suggested in the mechanism proposed by Modén et al.,[15] prompting our interest in studying it computationally. We should first note that the stereochemistry of the molecular mechanism whereby the H abstraction from RH occurs leads inevitably to the formation of intermediate **I**, with R· located in the middle of the channel and stabilized by interactions with ROH. If no O_2 is present in the vicinity to form ROO·, once the R· radical is formed, it can reorient in the AFI channel, approach a framework O atom, and bind to the framework. However, no direct bonding of R· to the framework upon the H transfer is possible without going through intermediate **I**, which is dictated by the stereochemistry of the process.

The energy diagram for the formation of a direct MnO−R bond is shown in Figure 7. In this case, the reaction coordinate was selected as the distance between the radical C atom in R· and the framework O atom to which R· will bind; this O is a nearest neighbor to Mn. The R· radical gradually approaches the framework O in an endothermic process, during which ROH is desorbed from Mn due to the steric repulsion with the approaching R·. The total activation energy for this process is 42 kJ/mol, after which a deep decrease in the energy takes place, yielding a final reaction enthalpy of −127 kJ/mol, which suggests a very high stability for the intermediate **U**. The formation of the O−C bond between R· and the framework results in an increase in the corresponding Mn−O distance (Figure 7-top, blue line).

The molecular structure of intermediate **U** is displayed in Figure 8. Upon binding of the R· radical, the framework O bends outward, toward the channel, so as to reduce the steric repulsion between the organic molecule and the framework walls (Figure 8, A). The C−O distance between the C atom and the framework O atom

dx.doi.org/10.1021/cs200401f |*ACS Catal.* 2011, 1, 1487–1497

(1.510 Å) is typical of a strong C−O single bond. The Mn−O bond distance to this O atom is longer (2.257 Å) than the other Mn−O bond distances (∼1.99 Å), a consequence of the new chemical properties of this O atom. In fact, the Mn^{II}−OR environment is similar to the Mn^{II}−OH Brønsted acid site of reduced Mn^{II} in AlPOs.

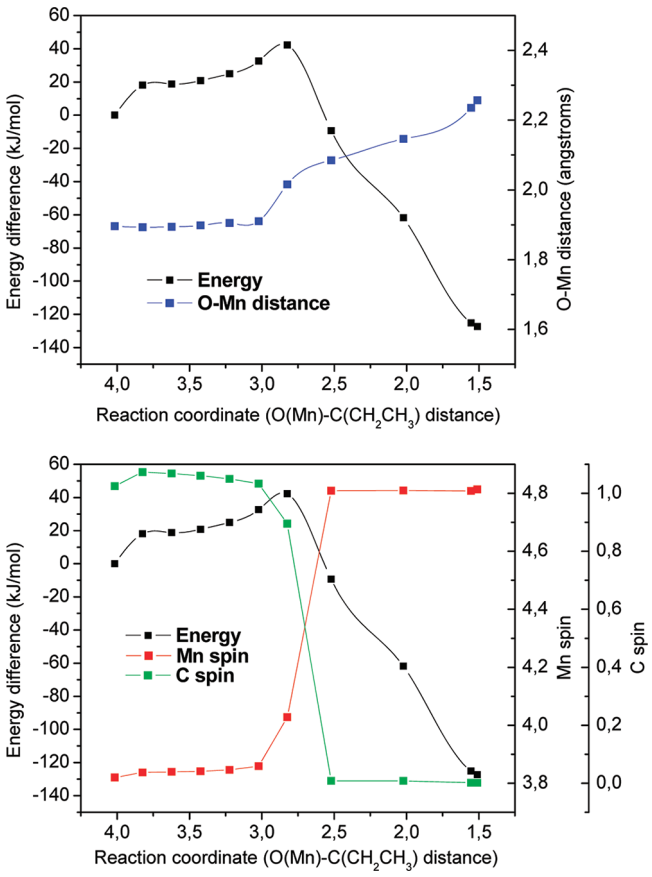

Figure 7. Top: Energy diagram (black line) and evolution of the O−Mn distance (blue line) along the reaction coordinate (represented as the distance between the radical C atom in CH_3CH_2· and the framework O atom bonded to Mn (O(Mn)−C(CH_2CH_3) distance) for the formation of a bond between the ethyl radical and the framework O (**I** → **U**). Bottom: Energy diagram (black line) and evolution of the C (green line) and Mn (red line) spin along the reaction.

Figure 7 (bottom) shows the evolution of the spin-polarization of the different species. Througout the reaction, the C spin decreases from 1 to 0, with a simultaneous increase in the Mn spin from 3.84 to 4.81. These results show that the unpaired electron initially present in the C atom of R· is transferred to Mn, which is reduced from Mn^{III} to Mn^{II}. The reduction of Mn is confirmed by the increase not only of the Mn−OR bond distance to 2.257 Å, but also of the other 3 Mn−O bond lengths from ∼1.91 to 1.99 Å as a result of the larger size of Mn^{2+} compared with Mn^{3+}. The one-electron transfer from C to Mn is also apparent from the spin density maps displayed in Supporting Information Figure 1. The spin-density is localized both on the Mn site and on the C atom of the ethyl radical in the reactants and in the TS, whereas in the products (**U**), spin density is localized only on the Mn active site and, indeed, increases from ∼4 (Mn^{3+}, d^4) to ∼5 (Mn^{2+}, d^5).

The reaction step examined here requires an activation energy of 42 kJ/mol. In contrast, the competing direct addition of O_2 to the R· radical previously discussed (**I** → **J**) required no activation and is even more exothermic (−141 kJ/mol, vs −127 kJ/mol), suggesting that the oxidation pathway will take place not through the Mn^{II}···R complex (**U**), but through the direct addition of O_2 to the free R· radical, provided O_2 is present in the channels. Even if complex **U** were formed, this intermediate should evolve by a subsequent addition of O_2 to produce ROO·; for the sake of completeness, this process was studied computationally and is reported in the Supporting Information (Figure 2-SI). Such an attack by O_2 requires a very high activation energy (∼170 kJ/mol), since it involves a dissociation of the stable C−O bond between R and the framework O in **U** (see Figure 2-SI, blue line), and requires decomposition of the very stable Mn^{II}···R complex. Furthermore, it is an endothermic process (+70 kJ/mol), since it involves a reoxidation of Mn^{II} to Mn^{III}, the least stable oxidation state, resulting in a free peroxo ROO· radical and a free Mn^{III} site (**K**). Therefore, if complex **U** were formed, it would not react further due to its stability, resulting in the deactivation of the active site, thus ruling out an extensive occurrence of this alternative mechanism in the oxidation pathway for both thermodynamic and kinetic reasons.

B. Propagation from Mn^{III}···OH (L → M → N → K). The least stable mode of adsorption of the hydroperoxide intermediate on Mn^{II} sites involves the formation of an H bond between the framework proton and the nonterminal O atom in ROOH, which leads to the formation of the Mn^{III}···OH

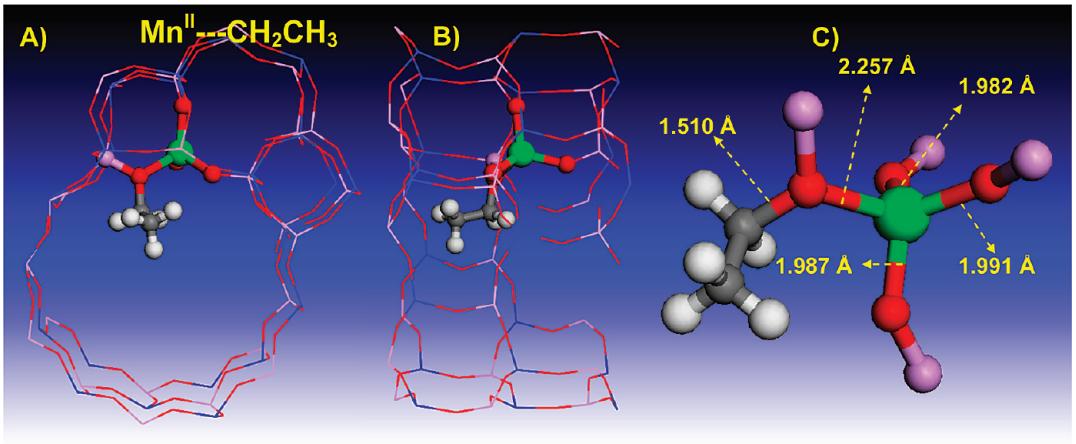

Figure 8. Two views (A and B) and detail (C) of the structure of intermediate **U**.

dx.doi.org/10.1021/cs200401f |*ACS Catal.* 2011, 1, 1487–1497

complex **L**. We then repeated the previous calculations for this complex **L**.

*B.1. H Transfer from RH to $Mn^{III}\cdots OH$ (**L** → **M**).* The radical-like nature of the HO· ligand in **L** allows a propagation reaction to occur by means of H abstraction from a new hydrocarbon molecule to form a water molecule. Supporting Information Figure 3 shows the energy diagram for this H-transfer reaction (left). In this case, we found that no activation energy is required for the H transfer. This process has an exothermic reaction enthalpy of −70 kJ/mol. As in section A.1, the evolution of the spin polarization of the different species along the reaction (Figure 3-SI, right) confirms the lack of any redox process involving the Mn sites (red line), and the negative spin of −1 of the hydroxo O atom present in complex **L** (pink line) is transferred to the C atom of RH (green line), resulting in the formation of a closed-shell H_2O molecule and an R· radical species in intermediate **M**. Spin-density maps similar to those of Figure 5 (for **H** → **I** step) were found (Supporting Information Figure 4) in which the β spin-density of O is transferred to C. These observations confirm that the dissociation of the C−H bond of the hydrocarbon is homolytic also in this case.

The molecular structure of the products (**M**) resulting from this elementary step is shown in Figure 5 of the Supporting Information. The intermediate **M** in this reaction is equivalent to **H** in section A, differing only in the product of the H-transfer reaction: in pathway A, this is an ROH molecule, but here, it is an HOH. In both cases, **H** and **M**, we observe an interaction between R· and the H atom that has been transferred, and the ethyl radical formed is strongly associated with the active site, rather than free inside the channel.

*B.2. O_2 Addition to R· (**M** → **N**).* Rapid addition of O_2 to the highly reactive R· radical to form a free peroxo radical ROO· is the next step. The addition of O_2 from intermediate **M** has features that are common to the reaction step **I** → **J** discussed in section A.2. As before, the addition of O_2 takes place without significant activation barriers and in a stereospecific way (the attack of O_2 takes place from the left side in Figure 5-SI, B). This step is exothermic (−129 kJ/mol) and gives place to a peroxo free radical (ROO·) located in the middle of the channel (**N**).

As for the $Mn^{III}\cdots OR$ complex **H**, a propagation subcycle to produce further ROOH from RH and O_2 could take place from the intermediate **N** (**N** → **BB** → **L** → **M** → **N**) through H transfer from H_2O to ROO·. However, as for the pathway through **BA**, our calculations showed that the **BB** intermediate is very unstable, and again, geometry optimizations always resulted in the hydrogen atoms being transferred back to the HO· radical to yield H_2O, a consequence of the lower stability of the hydroxo radical compared with that of ROO· (the O−H bond energies of H_2O and ROOH, shown in Table 1, are 500 and 362 kJ/mol, respectively), thus also ruling out the occurrence of this alternative propagation subcycle.

The final desorption of the H_2O molecule from Mn^{III} leaves the active site free; this process involves an endothermic enthalpy of +69 kJ/mol (**N** → **K**). Such a desorption of H_2O yields intermediate **K**, which consists of a free peroxo radical (ROO·) and the Mn^{III} site, resulting in the same intermediate that is produced in the propagation reactions from $Mn^{III}\cdots OR$ complex **H**.

A mechanism that is equivalent to that of Figure 6 would be possible in this oxidation route by just replacing the ligand ROH with H_2O. However, since these ligands are not involved in the binding of R· to the framework, a similar energy profile would be expected for this reaction, and therefore, for the same reasons previously discussed, this route was also discarded from the oxidation mechanism.

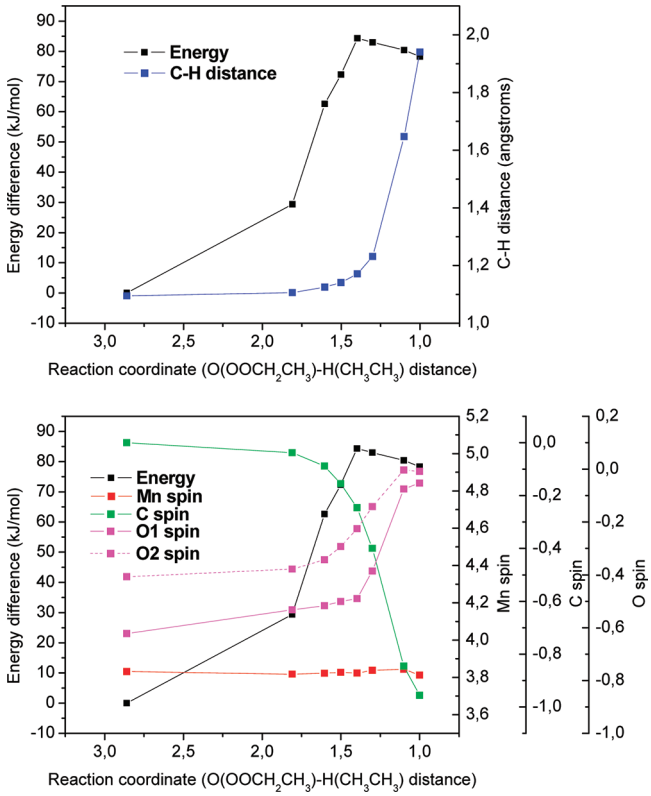

Figure 9. Top: Energy diagram (black line) and evolution of the C−H distance (blue line) along the reaction coordinate (represented as the distance between a H atom in CH_3CH_3 and the O atom in OOR ligand ($O(OOCH_2CH_3)$−$H(CH_3CH_3)$ distance) for the H transfer reaction from ethane to the peroxo ligand bonded to Mn^{III} (**O** → **P**). Bottom: Energy diagram (black line) and evolution of the C (green line), O (solid and dashed pink lines, corresponding to terminal (O1), and nonterminal (O2) O atoms, respectively), and Mn (red line) spin along the reaction.

C. Propagation Cycle from $Mn^{III}\cdots OOR$ (K → O → P → Q → K). The two mechanistic pathways explained above in sections A and B converge in intermediate **K**, where we have the free Mn^{III} site and a free peroxo radical in the middle of the channel. This free peroxo radical can be stabilized by approaching the nearby Mn^{III} free site and by forming the complex $Mn^{III}\cdots OOR$ (**O**), whose formation energy was calculated as −60 kJ/mol. This high stability is due to the Lewis acidity of the electron-defficient Mn^{III} (d^4) and the stabilization achieved by the peroxo radical upon complexation. Intermediate **O** is also a subproduct of the preactivation step, as shown in our previous work.[23] Further propagation cycles can start from this complex **O**.

*C.1. H Transfer from RH to $Mn^{III}\cdots OOR$ (**O** → **P**).* As in previous cases, the radical ROO· ligand can abstract a H atom from new hydrocarbon molecules. The energy profile for this H transfer is shown in Figure 9 (top). In this case, a relatively high activation energy of 84 kJ/mol is required for the H abstraction to take place. The H transfer involves dissociation of the C−H bond (blue line in Figure 9, top) and yields an ethyl radical R· and a hydroperoxide ROOH molecule that remains bonded to Mn^{III} (Supporting Information Figure 6); this process has an endothermic reaction enthalpy of +78 kJ/mol. The evolution of

dx.doi.org/10.1021/cs200401f |*ACS Catal.* 2011, 1, 1487–1497

the spin-polarization in the different species (Figure 9, bottom) shows again the lack of any redox process on Mn (red line). In this case, the spin polarization of the ROO· radical is shared between the two O atoms, which could explain the higher stability of these peroxo radicals (Table 1), although it is slightly more localized on the terminal O (O1) (pink line). Upon H transfer, the spin density of the two O atoms in ROO· is transferred to the C atom of the substrate RH, whose spin varies from 0 to −1 (green line), showing once again the homolytic nature of the C−H bond dissociation in the hydrocarbon, which is also apparent from the spin-density maps of this reaction (Supporting Information Figure 7).

C.2. O_2 Addition to R· (***P*** → ***Q***). As observed in previous sections, the ethyl radical R· is rapidly stabilized by the addition of O_2 to the radical C atom to form a free peroxo radical ROO·, which occurs without activation barriers and in a stereospecific way; consequently, the peroxo radical ROO· formed will be located in the middle of the channel (**Q**). As in previous cases, this addition of O_2 is exothermic (−154 kJ/mol). The spin-polarization of the ethyl radical R· is transferred from the C atom to the two molecular O atoms of O_2 (spin of 0.7 and 0.3).

Dissociation of complex **Q** yields free ROOH, able to enter the oxidation cycle through reaction with Mn^{II} (**F** → **L**/**H**), and a Mn^{III} free active site; this desorption energy was calculated as +52 kJ/mol (**Q** → **K**). Desorption of ROOH yields again intermediate **K**, therefore closing a propagation subcyle (**K** → **O** → **P** → **Q** → **K**) that involves the conversion of a hydrocarbon molecule and O_2 into a ROOH intermediate ($CH_3CH_3 + O_2 \rightarrow CH_3CH_2OOH$) that will re-enter the reaction cycle. This subcycle provides a preferential mechanistic pathway for the production of the hydroperoxide intermediate.

A propagation subcycle that is equivalent to those previously examined (**J** → **BA** or **N** → **BB**) is not possible in this case, since the two species where the H transfer would take place, ROO and ROOH, would lead to the same products as the reagents. Moreover, a mechanism similar to that of Figure 6 would also be possible in this mechanism, but for the same energetic reasons as before, this mechanism is to be discarded.

DISCUSSION

Our computational study has enabled us to identify the individual elementary steps responsible for the propagation phase of the catalytic cycle for hydrocarbon oxidations in MnAPO-5. The radical nature of the oxo-type ligands in complexes **H**, **L**, and **O** of ·OR, ·OH, and ·OOR with Mn^{III}, resulting from previous steps in the overall oxidation reaction, favors an H transfer from a hydrocarbon molecule to the radical O atoms, yielding in turn an ethyl radical. The reaction occurring at this stage can be expressed as $Mn^{III}\cdots OX + RH \rightarrow Mn^{III}\cdots HOX + R\cdot$. The calculated energies indicate that the H-abstraction ability of the three complexes follows the order $Mn^{III}\cdots OH$ (**L**) > $Mn^{III}\cdots OR$ (**H**) > $Mn^{III}\cdots OOR$ (**O**), which is explained by the different stabilities of the oxo radicals ·OH, ·OR, and ·OOR, as shown by the calculated O−H bond energies of HO−H (500 kJ/mol), RO−H (442 kJ/mol), and ROO−H (362 kJ/mol), respectively (Table 1).

The stability of the resulting oxo-type radicals follows the opposite order of the O−H bond energies. In turn, the lower the stability of the oxo radical, the higher its ability to abstract H in the Mn^{III} complex. The reaction enthalpy of the H-transfer step can be rationalized by comparing the O−H bond energies listed above with the energy of the C−H bond in RH that is cleaved in this elementary step (454 kJ/mol; see Table 1). ·OH radicals are less stable than R· radicals, explaining the highly exothermic nature of the H abstraction involving complex **L** ($Mn^{III}\cdots OH$) as well as the lack of any activation barrier.

In contrast, ROO· radicals are more stable, leading to the least favored H-abstraction process (**O** → **P**). The slightly exothermic nature of the H abstraction by complex **H** ($Mn^{III}\cdots OR$), despite R· and RO· having a bond energy similar to that of H, correlates to the stabilization achieved by R· through interaction with the H transferred (**I**), as observed in Figure 3, bottom. In all the mechanistic pathways originating from **H**, **L**, and **O**, the ethyl radical R· formed in the first step interacts with the Mn···HOX complex, but is not bonded directly to the framework. The radical C atom has a planar environment that is typical of sp^2 hybridization with the unpaired electron hosted in the "p" atomic orbital perpendicular to the CH_2 plane. The desorption energy of the R· radical from its interaction with the HOX ligand was found to be 22, 14, and 1 kJ/mol for HOH (**M**), ROH (**I**), and ROOH (**P**), respectively.

Once R· radicals are formed, the reaction proceeds via addition of O_2, which occurs in a stereospecific way due to the sterical impediment produced by the interaction of R· with the HOX ligand. The result is a peroxo radical ROO·, in which the unpaired electron is distributed over the two oxygen atoms, but more on the terminal (spin density of 0.7 |e| compared with 0.3 |e| in the nonterminal oxygen atom). The terminal O of the peroxo radical does not interact with the Mn dopant or with the HOX ligand formed in the previous reaction step and can therefore be considered as "free" within the AFI channels of the catalyst. Addition of O_2 to the R· radical causes the disappearance of the R−HOX interaction, explaining the difference in the reaction enthalpy observed starting from intermediates **L** ($Mn^{III}\cdots OH$; −129 kJ/mol), **H** ($Mn^{III}\cdots OR$; −141 kJ/mol), and **P** ($Mn^{III}\cdots OOR$; −154 kJ/mol). All three cases are exothermic due to the stability of the peroxo radical formed from ethyl + O_2; since the addition reaction is the same, the calculated reaction enthalpies indicate that the strength of the R·−HOX interaction decreases in the order: R·−HOH(Mn) > R·−HOR-(Mn) R·−HOOR(Mn), in turn due to the relative acidity of H in H_2O, ROH, and ROOH, in good agreement with the R· desorption energies shown previously. Even if the R· radicals are desorbed from the HOX ligand, a process which, though endothermic, is not very energy-demanding, especially for ROOH (1 kJ/mol) and ROH (14 kJ/mol), it would not alter the overall molecular mechanism, since the subsequent addition of O_2 to the free R· would yield the same free peroxo radical.

The next step in the propagation reactions involves the desorption of the neutral ligand formed following the H transfer, releasing the Mn^{III} site, which can bind the resulting ROO· and therefore continue the propagation cycle through complex **O** ($Mn^{III}\cdots OOR$). The dissociation energy for the three complexes $Mn^{III}\cdots OH_2$ (**N**), $Mn^{III}\cdots O(H)R$ (**J**), and $Mn^{III}\cdots O$-(H)OR (**Q**) follows the order H_2O (69 kJ/mol) > ROH (58 kJ/mol) > ROOH (52 kJ/mol), proportional to the Lewis basicity and the complexation ability of the three ligands.

Apart from the propagation steps discussed above, we have identified a catalytic subcycle (**K** → **O** → **P** → **Q** → **K**) that leads to the net production of ROOH from RH and O_2. The ROOH produced here sustains the propagation reaction by binding to an Mn^{II} site (**F**), which prompts its dissociation into intermediates **H** or **L**, depending on the stereochemistry of the ROOH adsorption.[24]

dx.doi.org/10.1021/cs200401f |*ACS Catal.* 2011, 1, 1487–1497

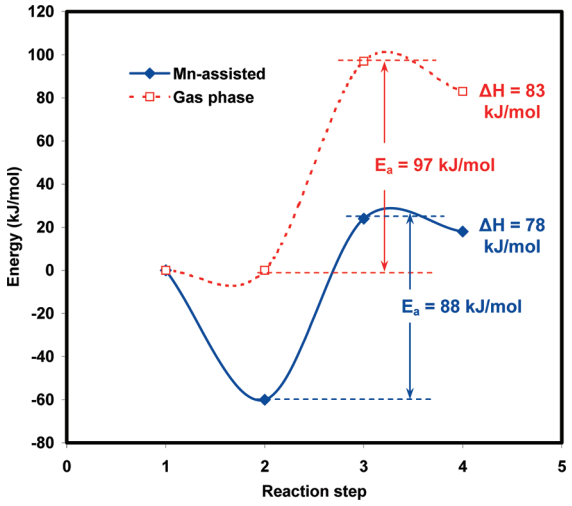

Figure 10. Energy profile for the H transfer from RH to ROO without the assistance of Mn (in gas phase, dashed red line) and with the assistance of Mn (blue line), showing the corresponding activation energies and reaction enthalpies.

ROOH production through this propagation subcycle requires an activation energy of 84 kJ/mol, which is considerably lower than that required through the preactivation route that also leads to the production of ROOH but with an activation energy of 135 kJ/mol.[23] The propagation subcycle through complex $Mn^{III}\cdots OOR$ identified here will therefore represent the main source of ROOH in the overall catalytic cycle, once the Mn sites have been preactivated, as previously suggested by Iglesia et al.[15]

The initial location of the peroxo radicals free inside the AFI channels (**K**) led us to consider the possibility that the subsequent transfer of H from RH to form ROOH could occur inside the pores but without the assistance of Mn, i.e. as in a gas-phase reaction (Figure 10). The free peroxo radical can follow two alternative paths: (i) it can approach an Mn^{III} free site and form a complex, a process that involves a reaction enthalpy of −60 kJ/mol (**O**), after which H transfer from RH will take place, with an activation energy of 84 kJ/mol and a reaction enthalpy of +78 kJ/mol; or alternatively, (ii) the H transfer can take place without binding to Mn, which involves a higher activation energy and reaction enthalpies of 97 and 83 kJ/mol. The high stabilization gained by the free peroxo radical upon binding to Mn (−60 kJ/mol), in contrast with the high activation energy required for the gas-phase H transfer (+97 kJ/mol), suggests that the free peroxo radical will, indeed, bind to Mn once it is formed and then undergo the H transfer assisted by Mn, implying that "gas-phase" propagation of ROO· will, if at all, be a minor process. Likewise, gas phase propagations from RO· and HO· are unlikely to occur, since in this case, the molecular mechanism of the ROOH decomposition leads to these radicals being already bonded to Mn, and their desorption from Mn demands a high energy cost (∼67 kJ/mol).[24]

We note that, in all the propagation reactions discussed above involving H transfers, O_2 additions, and complex dissociations, the role of Mn is indirect, because it enables the formation of complexes with the intermediates. However, no redox process involving Mn takes place, and Mn is always present as Mn^{III}.

The overall energy profile for the ROOH conversion into the oxidation products ROH and H_2O, including the ROOH decomposition discussed in our previous work[24] and the propagation

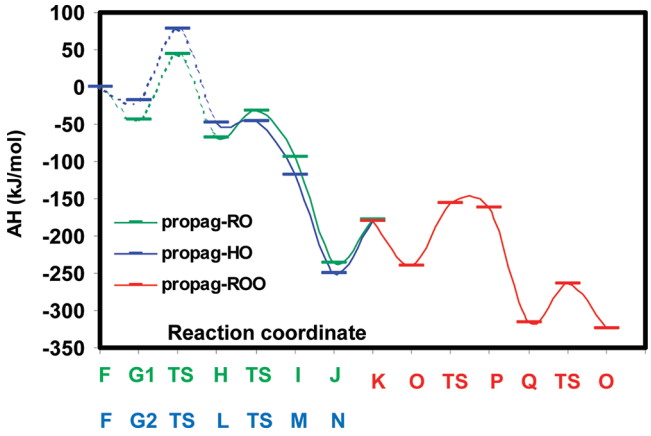

Figure 11. Energy profile for the overall process: ROOH decomposition (dashed line) + propagation reactions (solid line) through RO (green line), HO (blue line), and ROO (red line).

reactions discussed here, through the two alternative mechanistic routes, is summarized in Figure 11. Despite going through different intermediates, the two routes that convert ROOH into ROH and H_2O (green and blue lines in Figure 11 and Figure 1) involve the same net chemical transformations, starting from the same reactants (**F**) and ending with the same products (**K**). The net conversion achieved is $Mn^{II}(H) + ROOH + RH + O_2 \rightarrow H_2O + ROH + ROO\cdot + Mn^{III}$, which involves a net oxidation of Mn that must be reduced again to restart the cycle by means of the regeneration routes, whose mechanistic details will be published in a forthcoming paper. Since they involve the same overall chemical transformations, the net total energy associated with the two alternative mechanisms (sections A and B) must be the same, as, indeed, is the case (∼−180 kJ/mol; Figure 11). However, because of the different stability of the radical species involved, ·OH and ·OR, the energetic pathway is different in the two cases: the pathway through ·OR (green) involves a more favored decomposition of ROOH, and the H abstraction is less favorable, and the opposite occurs for pathway through ·OH (blue).

Finally, we discuss the implications of our mechanism for the regioselectivity of these oxidation reactions. Detailed investigation is precluded from the present study since we have used ethane as model for the hydrocarbon, where all the C atoms are primary. However, we consider that it is unlikely that the sequence of mechanistic steps will be modified with larger hydrocarbons. The mechanism and molecular structure of the intermediates identified here can therefore be used to give indications about regioselectivity, which is dictated by those steps in which the hydrocarbon is activated; namely, **H** → **I**, **L** → **M**, and **O** → **P**. As discussed, these H-transfer reactions take place from the hydrocarbon to an oxo-containing ligand (RO·, HO·, or ROO·) that is not free inside the channel, but bonded to the framework via Mn. Indeed, the ethyl radicals formed are also associated to the framework by interactions with the H atom of the HOX product which in turn is bonded to the framework via Mn. The large-pore and cylindrical nature of the AFI channels provides a weakly constrained space for the H abstraction from the hydrocarbon, resulting in the absence of any regioselectivity toward terminal oxyfunctionalisation as observed experimentally, since the interaction of the hydrocarbon molecule with the oxo-type ligand through a secondary or tertiary carbon atom does not

dx.doi.org/10.1021/cs200401f |*ACS Catal.* 2011, 1, 1487–1497

seem to be greatly sterically impeded (see Figure 3). Nevertheless, our proposed reaction mechanism clearly demonstrates that the H-transfer reactions that will determine the regioselectivity take place through radical-type oxo species that are bonded to Mn (**H**, **L**, and **O**). The detailed knowledge provided by our mechanistic study therefore gives useful guidance for the design of Mn−AlPO catalysts with improved regioselectivity control toward the desired terminal oxyfunctionalisation. Selection of appropriate framework geometries that enable a closer interaction between the species involved in the H abstraction and the framework could then be tailored.

CONCLUSIONS

In the present work, we have applied computational techniques to study the aerobic oxidation of hydrocarbons and focused on the propagation routes that transform the hydrocarbon molecules into the oxidation products, water and alcohol, and further hydroperoxide that will re-enter the oxidation cycle. The propagation reactions involve a series of H-abstraction, O_2-addition, and complex dissociation reactions performed by the complexes $Mn^{III}\cdots OH$, $Mn^{III}\cdots O$, and $Mn^{III}\cdots OOR$ ($M^{III}\cdots OX$).

Initial H abstraction from hydrocarbon molecules takes place due to the radical nature of the oxo ligands in the intermediates; these promote a homolytic dissociation of the C−H bonds and a consequent transfer of the hydrogen atom that is abstracted by the radical O atoms, resulting in a new O−H covalent bond. The different ability of the three complexes to perform such H abstraction is related to the relative stability of the radical oxo species involved: ·OH radicals are less stable, and so they provide the highest ability for H abstraction. The R· radicals formed are stabilized by interactions between the radical C atom and the transferred H atom belonging to the ligand, thus being associated with, but not directly bonded to, the framework. Such interaction makes the consequent addition of O_2 to the R· radicals occur in a stereospecific way, where O_2 binds to the radical carbon atom from the opposite side to the ligand, thus leading unavoidably to an ROO· radical located free inside the channel.

We also identified a catalytic subcycle that is able to yield ROOH intermediates, whose occurrence is highly favored through complexation to Mn. Indeed, this is the only role played by Mn in these propagation reactions: no Mn redox process is observed. The propagation route through the complex $Mn^{III}\cdots OOR$, which involves a net transformation of RH and O_2 into ROOH, requires a much lower activation energy than the corresponding transformation through the preactivation mechanism; the subcycle discussed here therefore provides the main source of ROOH during the oxidation reaction, once the Mn sites have been preactivated.

ASSOCIATED CONTENT

Supporting Information. Additional energy profiles, molecular structures, and spin density plots of several intermediates. This material is available free of charge via the Internet at http://pubs.acs.org/.

AUTHOR INFORMATION

Corresponding Author

*E-mail: (L.G.-H.) lhortiguela@icp.csic.es, (F.C.) f.cora@ucl.ac.uk.

ACKNOWLEDGMENT

L.G.-H. acknowledges funding from EPSRC (Grant EP/D504872). F.C. is supported by an RCUK Fellowship. We are grateful to Sir John Meurig Thomas, Gopinathan Sankar, and Claudio M. Zicovich-Wilson for helpful discussions. The authors acknowledge the use of the UCL Legion High Performance Computing Facility and associated support services in the completion of this work

REFERENCES

(1) Wilson, S. T.; Lok, B. M.; Flanigen, E. M. US Patent 4310440, 1982.
(2) Raja, R.; Thomas, J. M. *Chem. Commun.* **1998**, 1841–1842.
(3) Saadoune, I.; Corà, F.; Alfredsson, M.; Catlow, C. R. A. *J. Phys. Chem. B* **2003**, *107*, 3012–3018.
(4) Corà, F.; Sankar, G.; Catlow, C. R. A.; Thomas, J. M. *Chem. Commun.* **2002**, 734–735.
(5) Thomas, J. M. *Angew. Chem., Int. Ed.* **1999**, *38*, 3588–3628.
(6) Arends, I. W. C. E.; Sheldon, R. A.; Wallau, M.; Schuchardt, U. *Angew. Chem., Int. Ed. Engl.* **1997**, *36*, 1144–1163.
(7) Hartmann, M.; Ernst, S. *Angew. Chem., Int. Ed.* **2000**, *39*, 888–890.
(8) Thomas, J. M.; Raja, R.; Sankar, G.; Bell, R. *Nature* **1999**, *298*, 227–230.
(9) Modén, B.; Oliviero, L.; Dakka, J.; Santiesteban, J. G.; Iglesia, E. *J. Phys. Chem. B* **2004**, *108*, 5552–5563.
(10) Modén, B.; Zhan, B.-Z.; Dakka, J.; Santiesteban, J. G.; Iglesia, E. *J. Phys. Chem. C* **2007**, *111*, 1402–1411.
(11) Raja, R.; Sankar, G.; Thomas, J. M. *Angew. Chem., Int. Ed.* **2000**, *39*, 2313–2316.
(12) Vanoppen, D. L.; De Vos, D. E.; Genet, M. J.; Rouxhet, P. G.; Jacobs, P. A. *Angew. Chem., Int. Ed. Engl.* **1995**, *34*, 560–563.
(13) Luna, F. J.; Ukawa, S. E.; Wallau, M.; Schuchardt, U. *J. Mol. Catal. A: Chem.* **1997**, *117*, 405–411.
(14) Raja, R.; Sankar, G.; Thomas, J. M. *J. Am. Chem. Soc.* **1999**, *121*, 11926–11927.
(15) Modén, B.; Zhan, B.-Z.; Dakka, J.; Santiesteban, J. G.; Iglesia, E. *J. Catal.* **2006**, *239*, 390–401.
(16) Concepción, P.; Corma, A.; López-Nieto, J. M.; Pérez-Pariente, J. *App. Catal., A* **1996**, *143*, 17–28.
(17) Zhou, L.; Xu, J.; Chen, C.; Wang, F.; Li, X. *J. Porous Mater.* **2008**, *15*, 7–12.
(18) Dugal, M.; Sankar, G.; Raja, R.; Thomas, J. M. *Angew. Chem., Int. Ed.* **2000**, *39*, 2310–2313.
(19) Raja, R.; Sankar, G.; Thomas, J. M. *Chem. Commun.* **1999**, 829–830.
(20) Raja, R.; Thomas, J. M.; Sankar, G. *Chem. Commun.* **1999**, 525–526.
(21) Thomas, J. M.; Raja, R.; Sankar, G.; Bell, R. *Acc. Chem. Res.* **2001**, *34*, 191–200.
(22) Gómez-Hortigüela, L.; Corà, F.; Sankar, G.; Zicovich-Wilson, C. M.; Catlow, C. R. A. *Chem.—Eur. J.* **2010**, *16*, 13638–13645.
(23) Gómez-Hortigüela, L.; Corà, F.; Catlow, C. R. A. *ACS Catal.* **2011**, *1*, 18–28.
(24) Gómez-Hortigüela, L.; Corà, F.; Catlow, C. R. A. *ACS Catal.* **2011**, *1*, 945–955.
(25) Gómez-Hortigüela, L.; Corà, F.; Catlow, C. R. A. *ACS Catal.* **2011**, *1*, DOI: 10.1021/cs200402b.
(26) Dovesi, R.; Saunders, V. R.; Roetti, C.; Orlando, R.; Zicovich-Wilson, C. M.; Pascale, F.; Civalleri, B.; Doll, K.; Harrison, N. M.; Bush, I. J.; D'Arco, Ph.; Llunell, M. *CRYSTAL06*; University of Torino: Torino, 2006.
(27) Grimme, S. *J. Comput. Chem.* **2006**, *27*, 1787–1799.
(28) Ugliengo, P.; Zicovich-Wilson, C. M.; Tosoni, S.; Civalleri, B. *J. Mater. Chem.* **2009**, *19*, 2564–2572.